The Performance of a Zirconium-based Root Filling Material with Artifact Reduction Properties in the Detection of Artificially Induced Root Fractures Using Cone-beam Computed Tomographic Imaging

Aaron Fox, DDS, Bettina Basrani, DDS, PhD, FRCD(C),* and Ernest W.N. Lam, DMD, MSc, PhD, FRCD(C)†*

Abstract

Introduction: Limited field of view cone-beam computed tomographic (CBCT) imaging has been used to augment clinical testing of vertical root fractures (VRFs); however, the presence of gutta-percha (GP) in the canal space generates substantial imaging artifacts that make fracture detection difficult. The purpose of this study was to evaluate the influence of a zirconium (Zr)-based root filling material with radiologic properties that reduce beam hardening (BH) artifacts using CBCT imaging in the *in vitro* diagnosis of VRFs. **Methods:** One hundred seventy-six single-rooted mandibular premolar teeth were obtained, and half of these teeth were filled with GP or Zr (CPoint; EndoTechnologies, LLC, Shrewsbury, MA). VRFs were induced in 44 decoronated teeth in each group using an Instron (Norwood, MA) Universal Testing Machine. Each root was then placed in a dry human mandible and imaged with the Carestream 9000 3D CBCT system (Carestream Dental, Atlanta, GA). The images were evaluated by 6 oral maxillofacial radiologists (OMRs) and residents. **Results:** The sensitivity was greater for detecting VRFs in the Zr group than the GP group (P = .035). However, the specificity was greater for the GP group than the Zr group (P = .028). Receiver operating characteristic area under the curve values were greater for the Zr group than the GP group, but these differences were not statistically significant. The OMRs outperformed the residents in the detection of VRFs in the Zr group with respect to specificity (P = .006) and positive predictive value (P = .012). **Conclusions:** The reduced BH of the Zr group improved the sensitivity of the detection of artificially induced VRFs. The ability to detect VRFs in the Zr group was further enhanced by clinical experience. *(J Endod 2018;44:828–833)*

Key Words

Beam hardening artifact, cone-beam computed tomography, gutta-percha, vertical root fracture, zirconium

Significance

A zirconium-based root filling material with its reduced K absorption edge improved the sensitivity of vertical root fracture detection using CBCT imaging. Root filling materials with K edge values below 18.0 keV should be explored for continuing research in clinical endodontics.

A vertical root fracture (VRF) is defined as a plane of cleavage in a root that may occur buccolingually or mesiodistally (1). Clinical studies of extracted endodontically treated teeth with the presumption of VRFs suggest a prevalence of between 3% and 13% (2–6). VRFs develop primarily in response to wedging forces within the canal space, such as during post placement and cementation, or condensing root canal filling materials (7). Wedging forces, when excessive, can cause dentinal fatigue, resulting in the formation of material defects that may lead to fracture (8). This complication ultimately leads to tooth extraction.

The use of conventional imaging techniques for VRF detection is somewhat controversial. It has been shown with plain film imaging that to visualize a VRF the primary x-ray beam needs to be aligned to within 4° of the fracture plane (9). Moreover, the superimposition of adjacent anatomic structures makes visualization of a VRF even more difficult. Recently, high-resolution, limited field of view cone-beam computed tomographic (CBCT) imaging has been used to evaluate teeth in endodontic clinical practice with suspected VRFs. Although recent systematic reviews and met-analytic studies on this topic have reported moderate to high performance parameters of sensitivity and specificity (10), Chang et al (11) have noted significant biases in these data sets that question their reliability. Unfortunately, the visualization of fracture planes in teeth that have undergone endodontic and/or restorative procedures with highly dense materials such as gutta-percha (GP), metal posts, and crowns are prone to display image artifacts on CBCT images that can potentially mask abnormalities, including the visualization of fracture planes (12).

Artifacts produced in radiologic imaging represent discrepancies between the reconstructed image and the attenuation features of the actual physical object under

From the Graduate Programs in *Endodontics, and †Oral and Maxillofacial Radiology, Faculty of Dentistry, University of Toronto, Toronto, Ontario, Canada.

Address requests for reprints to Dr Aaron Fox, Graduate Program in Endodontics, University of Toronto, 124 Edward Street, Toronto, Ontario M5G 1G6, Canada. E-mail address: aafox1@gmail.com

0099-2399/$ - see front matter

https://doi.org/10.1016/j.joen.2018.02.007

investigation. A beam hardening (BH) artifact occurs when lower-energy x-ray photons in the polychromatic x-ray beam are absorbed by a high-attenuation or radiopaque material in preference to higher-energy photons. The result is that the attenuated x-ray beam exits the material with a higher mean energy than the primary beam (ie, it becomes "harder" and more intense) when it reaches the detector. This results in distortion of the attenuated x-ray beam because of the differential absorption (otherwise known as a "cupping" artifact) and produces streaks and dark bands between 2 adjacent radiopaque objects (13). BH artifacts in the CBCT image degrades image quality and compromises the diagnostic value of the image, making the identification of VRFs both challenging and time-consuming.

In an attempt to improve VRF detection, some CBCT system manufacturers and third parties have developed artifact reduction (AR) software to minimize or eliminate BH artifacts. These algorithms appear to reduce the effects of BH and scattering, increase the contrast-to-noise ratio, and decrease pixel gray value variation on the images (14). The major drawback of these algorithms is incomplete artifact correction, and, indeed, some even produce secondary artifacts (15). Some studies report that the algorithm can sometimes negatively alter an image. For example, when imaging teeth in which root canals have been filled with GP, part of the periphery of the GP can go "missing" compared with an image without AR. This "improper" reduction of artifacts can further accentuate diagnostic difficulties (15).

Modern GP cones are composed of inorganic components such as zinc oxide and barium sulfate, and the proportions of these contribute to the radiopacity of the material (16). Recently, EndoTechnologies LLC (Shrewsbury, MA) has produced a zirconium (Zr) root filling material with a central core comprised of a Zr particle suspension, which imparts different radiologic properties relative to conventional GP (17). The Zr atom absorbs or attenuates less of the incident x-ray beam through the material because of its lower K absorption edge (18.0 keV). Compared with barium, which has a K absorption edge of approximately 37.4 keV, Zr is a weaker radiologic attenuator for the mean energy of the polychromatic intraoral x-ray beam (approximately 33 keV) (18). Because the barium atom in the barium sulfate component of GP has a higher K absorption edge, barium is a stronger attenuator of the incident x-ray beam than Zr.

The aim of this study was to determine the ability to detect artificially induced VRFs using CBCT imaging in a single root canal–treated tooth with a conventional GP root filling material (Tulsa Dentsply Sirona, Tulsa, OK) versus a Zr root filling material (EndoTechnologies, LLC). Furthermore, the reduction in artifact production from the zirconium-based material on CBCT images may enable more reliable interpretation of VRFs in endodontically treated teeth.

Materials and Methods

An *a priori* power analysis was performed, and it was determined that a total of 176 teeth would be required to attain 80% confidence with the limits of a 2-sided 90% confidence interval to exclude a difference between visualizing and not visualizing VRFs of more than 25% (effect size). This study was independently reviewed and approved by the Human Research Ethics Board at the University of Toronto, Toronto, Ontario, Canada.

One hundred seventy-six extracted human single-rooted mandibular premolar teeth and 1 dry human mandible were used for this investigation. The extracted teeth were obtained from the Oral and Maxillofacial Surgery Clinic in the Faculty of Dentistry, University of Toronto and stored until use in formalin. The teeth were inspected to ensure that the roots were uniformly straight and conical in shape. All tooth roots with asymmetric curvature were excluded as were those that had been previously endodontically treated. The teeth were further inspected with the aid of a surgical operating microscope (Zeiss Meditec AG, Jena, Germany) using fiberoptic transillumination (Microlux Transilluminator; Addent, Danbury, CT) to exclude teeth with VRFs.

All 176 teeth were decoronated at the level of their cementoenamel junctions using a double-sided diamond disk (NTI Flex; Kerr Dental, Orange, CA). All canal systems were evaluated by using the surgical operating microscope under 10× magnification after decoronation. This permitted visualization of the root canal system to the apex in its entirety. Moreover, the shaping process was also conducted under high magnification for all samples. Canals were initially negotiated and patency confirmed with a 10 K-file (Flexofile, Tulsa Dentsply Sirona). The canals were instrumented using rotary files (Vortex, Tulsa Dentsply Sirona) according to the manufacturer's instructions up to a 45.06 master apical file and irrigated with 2% sodium hypochlorite (Clorox Company, Oakland, CA) between the introduction of each instrument with a 30-G needle (Tulsa Dentsply Sirona) 2 mm from the working length.

The prepared teeth were divided into 2 root filling groups: GP and Zr (Fig. 1). For the GP group (n = 88), 45.06 GP (Vortex GP, Tulsa Dentsply Sirona) points were placed, and for the Zr group (n = 88) 45.06 Zr (CPoint, EndoTechnologies, LLC) points were used. All of the points were inserted into the prepared root canals 0.5 mm short of the working length with a light application of EndoSequence BC Sealer (Brasseler, Savannah, GA) using the single-cone technique. All orifices were sealed with a thin layer of composite resin (Filtek Bulk; 3M ESPE, St Paul, MN).

Forty-four teeth in the GP group and 44 teeth in the Zr group were imaged without being subjected to the fracture protocol. Eighty-eight teeth (44 from each fill group) were embedded in a layer of baseplate wax (Patterson Baseplate Wax; Patterson Dental Supply, St Paul, MN), surrounded by microstone within a copper tube cap (13-mm diameter × 20-mm height), and placed on a fixed platform of an Instron (Norwood, MA) Universal Testing Machine. The machine was programed for the crosshead to apply a force at 1 mm/min until a drop in force by 20% was recorded, suggesting a fracture (17). The tooth was then removed from the matrix and inspected using a surgical operating microscope (Zeiss Meditec AG) at 10– magnification to verify the presence of a VRF.

Micro–computed Tomographic Evaluation

Three representative samples each from the GP and Zr groups also underwent micro–computed tomographic (micro-CT) (μCT 40; SCANCO Medical AG, Bruttisellen, Switzerland) scanning to investigate fracture width, variations in fracture pattern, and extension. Imaging was performed at a voxel resolution of 18 μm, and 3 regions of interest were systematically selected from the midpoints of each third of the root canal (ie, midcoronal, midmiddle, and midapical). The axial sections were uploaded into ImageJ software (National Institutes of Health, Bethesda, MD) (15), and fracture widths were measured at the external root surface and at the widest region of the fracture (Fig. 2).

CBCT Imaging

A reproducible jig was manufactured that was secured onto the platform of a Carestream 9000 3D (Carestream Dental, Atlanta, GA) CBCT unit. The lower border of a dried human mandible was fixed to the surface of the bite plane with Krazy Glue (Krazy Glue, Westerville, OH) and polyvinyl siloxane impression material (President; Coltene/Whaledent AG, Alstatten, Switzerland). The mandible was positioned so that the long axis of the tooth under investigation was oriented perpendicular to the supporting platform. A 5-mm thickness of baseplate wax (Patterson Baseplate Wax) was placed around the body of

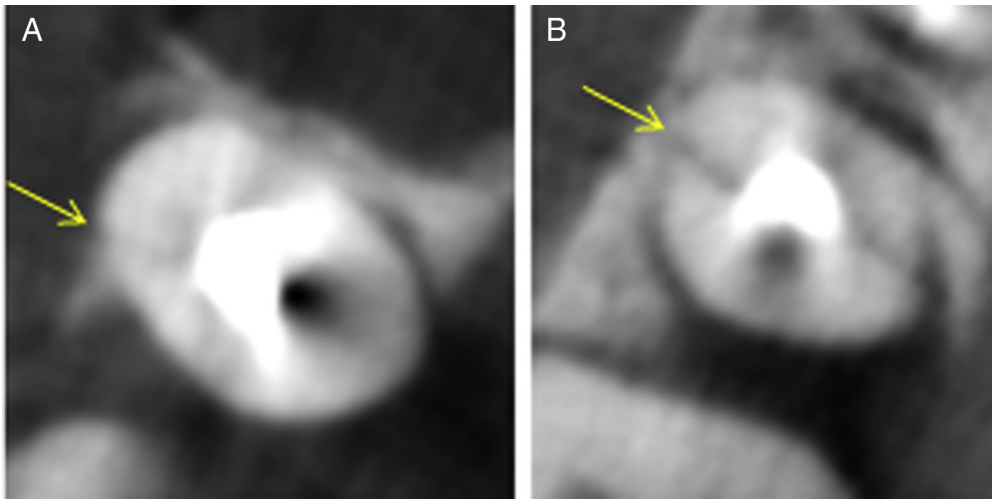

Figure 1. A cross section through the coronal root region demonstrating the extent of the beam hardening artifact. (*A*) Produced by a GP sample with a crack (*yellow arrow*). (*B*) Produced by a Zr sample with a crack (*yellow arrow*).

the mandible to mimic soft tissues. Volume acquisitions were made at 70 kVp, 3.2 mA, and 76-μm voxel size resolution with a limited field of view (5-cm diameter × 3.7-cm height).

Six examiners (4 oral and maxillofacial radiology residents [RRs] and 2 certified oral maxillofacial radiologists [OMRs]) independently assessed the CBCT volumes of the teeth for VRFs. Examiners were calibrated before the imaging assessment using a subset of the image volumes. The Digital Imaging and Communications in Medicine data were viewed using Carestream CS 3D Imaging software (Carestream Dental) on Dell S2340Lc monitors (Dell, Round Rock, TX) in a quiet room under low ambient light. A VRF was defined as a vertical or oblique low-attenuation/radiolucent plane running through the long axis of the root. For each of the 176 teeth, the examiners were asked to score the absence or presence of VRFs.

Statistical Analysis

The observers' responses were recorded using an Excel (Microsoft, Redmond, WA) spreadsheet. The data were analyzed using SPSS software (SPSS version 24; IBM Corp, Armonk, NY). The null hypothesis was rejected when P was $< .05$.

Inter- and intraobserver agreements were assessed for all examiners using the Cohen kappa, and agreement was interpreted as being slight (0.00–0.20), fair (0.21–0.40), moderate (0.41–0.60), substantial (0.61–0.80), almost perfect (0.81–0.99), and perfect (1.00). Interobserver agreement was also assessed using the Fleiss kappa for the 2 groups of observers, and this was calculated separately for the GP and Zr groups and for both materials combined.

The diagnostic abilities of the observer groups were assessed for each material by creating receiver operating characteristic curves and by calculating the area under the curve. This was done for all observers as a group and separately (ie, RRs and OMRs). A 2-point scale was used to indicate the absence or presence of a fracture. The sensitivity, specificity, positive predictive value (PPV), negative predictive value (NPV), and accuracy values were compared by the paired t test for the pooled observer data and by the independent t test for each observer group.

Results

Six teeth underwent micro-CT imaging to characterize the fracture model. The fracture width of the 3 samples in the GP group ranged from 0.033–0.245 mm in the coronal region of the root and 0.018–0.094 mm in the middle one third of the root, and there were no fracture extensions to the apical thirds of the samples evaluated. All fractures involved the coronal thirds of each root, whereas only 2 out of 3 fractures extended into the middle third. Incomplete fractures were identified in 1 out of 3 samples and complete fractures in 2 out of 3 samples.

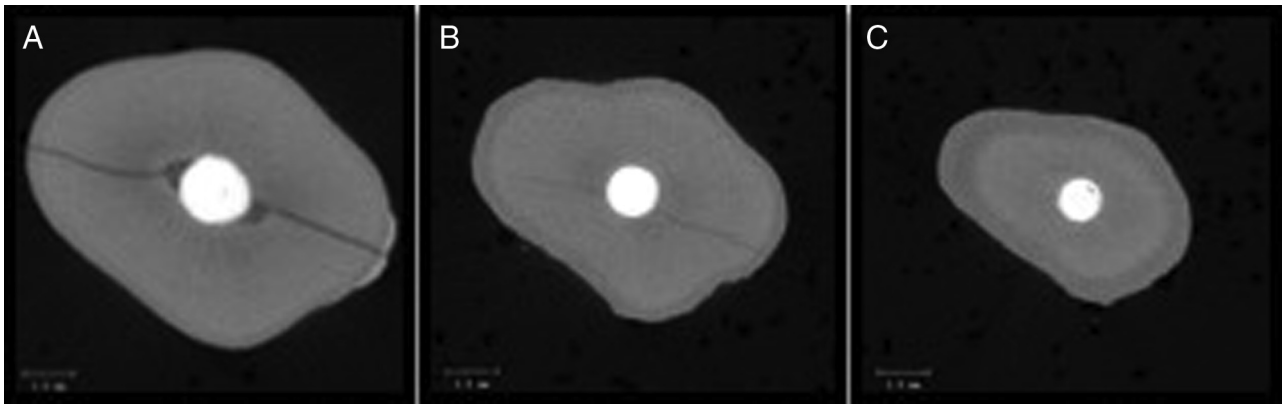

Figure 2. A micro-CT image of a Zr-filled tooth. (*A*) The midcoronal axial region showing a complete fracture pattern. (*B*) The midmiddle axial region showing an incomplete fracture pattern. (*C*) The midapical axial region showing no fracture present.

TABLE 1. Diagnostic Performance for All Observers for the Detection of Vertical Root Fractures

Diagnostic characteristics	Gutta-percha material	Zirconium material	Mean difference, 95% CI	Paired sample *t* test
Sensitivity	46.59 ± 14.14	58.33 ± 12.50	11.74 (1.24–22.24)	$t_5 = -2.88$, $P = .035$
Specificity	84.85 ± 10.33	73.86 ± 14.07	10.99 (1.76–20.22)	$t_5 = 3.06$, $P = .028$
PPV	74.96 ± 13.26	71.34 ± 11.07	3.62 (−2.79 to 10.03)	$t_5 = 1.45$, $P = .206$
NPV	61.76 ± 8.56	64.44 ± 4.70	−2.68 (−9.08 to 3.73)	$t_5 = -1.07$, $P = .332$
Overall accuracy	65.72 ± 9.60	66.10 ± 3.90	−0.38 (−8.28 to 7.52)	$t_5 = -0.12$, $P = .906$

CI, confidence interval; NPV, negative predictive value; PPV, positive predictive value.
The reported values represent percentages in a format of mean ± standard deviation.

The fracture widths of 3 samples in the Zr group ranged from 0.144–0.297 mm in the coronal region of the root, 0.054–0.161 mm in the middle third of the root, and 0.051 mm in the apical region. All fractures involved the coronal thirds of each root, whereas only 1 out of 3 fractures extended into the middle or apical thirds of each root. Incomplete fractures were identified in 1 out of 3 samples and complete fractures in 2 out of 3 samples.

In the observer study, the intraobserver agreement was "almost perfect" (0.90) for the diagnosis of VRFs. Using the Cohen kappa test, the interobserver agreement ranged from 0.15 (slight)–0.65 (substantial) for the GP group and 0.22 (fair)–0.41 moderate for the Zr group for all examiners. Using the Fleiss kappa test, the interobserver reliability for the OMRs was 0.35 (fair) for GP, 0.66 (substantial) for Zr, and 0.51 (moderate) for both materials combined. For the residents, the interobserver reliability was 0.32 (fair) for GP, 0.22 (fair) for Zr, and 0.30 (fair) for both materials combined.

The diagnostic performance values for all examiners are summarized in Table 1. Statistically significant differences were found for the sensitivity ($P = .035$) of root fracture detection for the Zr group and specificity ($P = .028$) for the GP group. There were no significant differences in the PPV ($P = .206$), NPV ($P = .332$), or accuracy ($P = .906$) for either material. Furthermore, there were no differences for the area under the curve between the 2 materials or for the individual observer groups.

Table 2 summarizes the diagnostic performance values between the RRs and the OMRs. No statistical differences were found between the RRs and the OMRs for the GP-filled teeth. However, statistically significant differences were found for the OMRs with respect to specificity ($P = .006$) and PPV ($P = .012$) compared with the RRs for the Zr-filled teeth.

Discussion

Recently, CBCT imaging has been used to augment clinical testing for the diagnosis of VRFs in endodontic clinical practice. However, it is now well-documented that GP within the canal space generates substantial BH artifacts that degrade the quality of the images to the point of making fracture detection difficult, if not impossible.

Numerous authors have addressed a variety of different parameters that may dictate the accuracy of VRF detection (*ex vivo*) using CBCT imaging including different CBCT devices; technical factors such as voxel size, kVp, and/or mA; system-specific imaging modes; AR algorithms; commercial software packages and applications capable of Digital Imaging and Communications in Medicine display; and varying fracture widths (14, 15, 19–25). Previously, we have conducted an observer performance study of 5 oral and maxillofacial radiology graduate students' and certified oral and maxillofacial radiologists' abilities to detect VRFs in nonendodontically treated teeth and have reported sensitivity and specificity values of 64.0% and 70.6% (26). However, this was neither the aim nor the hypothesis of the current study. Rather, this is a materials performance study, addressing the influence of a novel root filling material with reduced BH artifact properties on vertical fracture detection compared with what has been the convention in clinical endodontics—GP.

The presence of barium in GP substantially impacts the radiopacity of the material on x-ray–based imaging because of its relatively high K absorption edge value (37.4 KeV) (18). The K absorption edge is the binding energy of the innermost K shell electrons orbiting the nucleus of an atom. As the energy of the incident x ray approaches the binding energy of a K shell electron, it is preferentially absorbed through the photoelectric effect, and transmission of the incident x-ray decreases. Moreover, as the K absorption value increases, the number of transmitted photons decreases (18). The mean x-ray beam energy of an intraoral x-ray beam operating between 65 kVp and 70 kVp is approximately 33 keV. Because the barium in GP has a K absorption edge of 37.4 keV, it is a much better absorber of this radiation than Zr, which has a K absorption edge of 18.0 KeV. Therefore, the weaker attenuating Zr creates less beam hardening as it exits the root. We have

TABLE 2. Diagnostic Performance of Certified Oral and Maxillofacial Radiologists and Oral Radiology Residents for the Detection of Vertical Root Fractures

Diagnostic characteristics	Oral radiologists	Radiology residents	Mean difference, 95% CI	Independent sample *t* test
Gutta-percha material				
Sensitivity	40.91 ± 0.00	49.43 ± 17.35	−8.52 (−44.64 to 27.50)	$t_4 = -0.66$, $P = .548$
Specificity	94.32 ± 4.82	80.11 ± 8.97	14.20 (−5.36 to 33.76)	$t_4 = 2.02$, $P = .114$
PPV	88.28 ± 9.14	68.31 ± 9.37	19.98 (−2.41 to 42.36)	$t_4 = 2.48$, $P = .068$
NPV	61.47 ± 1.21	61.91 ± 11.02	−0.44 (−23.44 to 22.55)	$t_4 = -0.05$, $P = .960$
Overall accuracy	67.62 ± 2.41	64.77 ± 12.17	2.85 (−22.66 to 28.35)	$t_4 = 0.31$, $P = .772$
Zirconium material				
Sensitivity	46.59 ± 1.61	64.20 ± 11.04	−17.62 (−40.68 to 5.44)	$t_4 = -2.12$, $P = .101$
Specificity	90.91 ± 6.43	65.34 ± 5.04	25.57 (12.54–38.60)	$t_4 = 5.45$, $P = .006$
PPV	84.34 ± 9.28	64.84 ± 2.56	19.50 (7.14–31.86)	$t_4 = 4.38$, $P = .012$
NPV	62.96 ± 0.95	65.17 ± 5.86	−2.21 (−14.47 to 10.05)	$t_4 = -0.50$, $P = .643$
Overall accuracy	68.75 ± 2.40	64.77 ± 4.05	3.98 (−4.93 to 12.89)	$t_4 = 1.24$, $P = .283$

CI, confidence interval; NPV, negative predictive value; PPV, positive predictive value.

recently developed a novel method that objectively quantifies the 2 elements of the BH artifact: the so-called "dark" and "light" artifacts. In this study, we evaluated the contribution of both the dark and light components of the BH artifacts in 3 regions of the tooth roots treated with conventional GP and the Zr filling materials (27). We reported a statistically significantly greater contribution of the dark artifact produced by GP (which has a higher K absorption edge) than the Zr-based material in all regions of the tooth root ($P < .05$). A statistically significant difference was also found between all 3 regions of the tooth roots for the light artifact ($P < .001$), and we concluded that the use of a root canal filling material with a lower K absorption edge can reduce BH artifacts along the length of the root canal.

Maximizing sensitivity and specificity are important features of a diagnostic test. In the present study, the overall sensitivity was higher in the Zr group (58.33%) compared with GP (46.59%), and this difference was found to be statistically significant. In general, our reported sensitivity values are relatively low but comparable with a recent study in which "resident" observers were used in the image interpretation process (19). The lower sensitivity values may also be explained by the widths of the fractures that were induced. Another parameter that may explain the lower sensitivity values among material groups was the use of lower kVp and mA exposure settings (70k Vp and 3.2 mA), which intended to simulate *in vivo* imaging practices. Furthermore, the finding of the higher sensitivity for the Zr group suggests that if there is a VRF in a Zr-filled tooth, the higher sensitivity provides greater confidence for ruling the VRF out. The current study also found a statistically significant difference in specificity values between the GP (84.85%) and Zr (73.86%) groups. A higher specificity implies that when a fracture is identified on CBCT images in a root canal filled with GP, the clinician can be more confident that the fracture is real.

Previous studies have confirmed that smaller fracture widths and incomplete fracture patterns are associated with a reduced diagnostic ability (19, 25). In the current study, we used micro-CT imaging to account for these variations in our observer data. We found that fracture planes could be consistently generated in the coronal thirds of the GP and Zr-filled roots and that fewer fracture planes extended into the middle and apical thirds of the roots. These results suggest fracture identification may be more difficult more apically. Furthermore, in order for a fracture to be identifiable, it must traverse at least 2 voxel widths (in our case, 152 μm). In our model, we were able to achieve this threshold only in the coronal portions of the roots where the amount of filling material is greatest. Therefore, our micro-CT data would suggest that fractures may be the most easily identifiable in the coronal thirds of roots unless large, metallic coronal restorations are present. In other areas of the root, CBCT systems with even the smallest-sized voxels may be incapable of demonstrating the fracture plane.

The value of a diagnostic test is not only influenced by sensitivity and specificity but also by the false-negative and false-positive rates produced. The OMRs showed a markedly lower false-positive rate for both root filling material groups compared with the RRs (2.3%–14% range vs 9%–36% range, respectively). The OMRs outperformed the RRs across all diagnostic parameters except for 2, sensitivity and NPV for the Zr group. Interestingly, statistically significant differences were found between the 2 groups for specificity and PPV within the Zr material group only. Because Zr is associated with less BH artifacts, visual features of the image such as contrasts at edges, shapes, and textures may attract attention without conscious processing (28). Expert observers also have a speed advantage in diagnostic interpretation because larger amounts of information can be recognized rapidly, whereas the inexperienced observer may have to rely on image fixation without higher cognitive feedback. This has been shown in studies that evaluated differences in eye movement patterns across an image between expert observers and resident trainees. Experts spend less time gazing at a particular image feature and have fewer rapid eye movements across the image. Moreover, experts also make use of their peripheral vision in the search process unlike resident trainees (25).

Conclusion

The Zr root-filling material may improve the sensitivity of the detection of artificially induced VRFs. Our study also supports the value of observer experience in the detection of VRFs because certified OMRs outperformed RRs. Our results should also encourage further research in the material and radiologic properties of novel root filling materials in the era of CBCT imaging.

Acknowledgments

The authors are grateful to the Oral and Maxillofacial Radiology Clinic at the University of Toronto (Toronto, Canada) for its support of the study.

Supported by the Alpha Omega Foundation, the Canadian Academy of Endodontics Foundation, and the Dr Lloyd and Mrs Kay Chapman Chair in Clinical Sciences.

The authors deny any conflicts of interest related to this study.

References

1. *American Association of Endodontists*. Chicago, IL: Glossary of Terms; 2017.
2. Testori T, Badino M, Castagnola M. Vertical root fractures in endodontically treated teeth: a clinical survey of 36 cases. J Endod 1993;19:87–91.
3. Torbjorner A, Karlsson S, Odman PA. Survival rate and failure characteristics for two post designs. J Prosthet Dent 1995;73:439–44.
4. Tamse A, Fuss Z, Lustig J, Kaplavi J. An evaluation of endodontically treated vertically fractured teeth. J Endod 1999;25:506–8.
5. Moule AJ, Kahler B. Diagnosis and management of teeth with vertical root fractures. Aust Dent J 1999;44:75–87.
6. Landys Boren D, Jonasson P, Kvist T. Long-term survival of endodontically treated teeth at a public dental specialist clinic. J Endod 2015;41:176–81.
7. Rivera E, Walton R. *Longitudinal Tooth Cracks and Fractures: An Update and Review*. Hoboken, NJ: John Wiley & Sons Ltd; 2015:14–42.
8. Kishen A. *Biomechanics of Fractures in Endodontically Treated Teeth*. Hoboken, NJ: John Wiley & Sons Ltd; 2015:3–13.
9. Kositbowornchai S, Nuansakul R, Sikram S, et al. Root fracture detection: a comparison of direct digital radiography with conventional radiography. Dentomaxillofac Radiol 2001;30:106–9.
10. Talwar S, Utneja S, Nawal RR, et al. Role of cone-beam computed tomography in diagnosis of root fractures: a systematic review and meta-analysis. J Endod 2016; 42:12–24.
11. Chang E, Lam E, Shah P, Azarpazhooh A. Cone-beam computed tomography for detecting vertical root fractures in endodontically treated teeth: a systematic review. J Endod 2016;42:177–85.
12. Bernardes RA, de Moraes IG, Hungaro Duarte MA, et al. Use of cone-beam volumetric tomography in the diagnosis of root fractures. Oral Surg Oral Med Oral Pathol Oral Radiol Endod 2009;108:270–7.
13. Barrett JF, Keat N. Artifacts in CT: recognition and avoidance. Radiographics 2004; 24:1679–91.
14. de Rezende Barbosa GL, Sousa Melo SL, Alencar PN, et al. Performance of an artefact reduction algorithm in the diagnosis of *in vitro* vertical root fracture in four different root filling conditions on CBCT images. Int Endod J 2016;49:500–8.
15. Bechara B, Alex McMahan C, Moore WS, et al. Cone beam CT scans with and without artefact reduction in root fracture detection of endodontically treated teeth. Dentomaxillofac Radiol 2013;42:20120245.
16. Maniglia-Ferreira C, Gurgel-Filho ED, de Araujo Silva JB Jr, et al. Chemical composition and thermal behavior of five brands of thermoplasticized gutta-percha. Eur J Dent 2013;7:201–6.
17. EndoTechnologies, LLC. Available at: http://endotechnologies.com/. Accessed July 30, 2017.
18. Curry TSI, Dowdey JE, Murray RC Jr. *Christensen's Introduction to the Physics of Diagnostic Radiology*, 3rd ed. Philadelphia: Lea & Febiger; 1984.
19. Patel S, Brady E, Wilson R, et al. The detection of vertical root fractures in root filled teeth with periapical radiographs and CBCT scans. Int Endod J 2013;46:1140–52.
20. Hassan B, Metska ME, Ozok AR, et al. Comparison of five cone beam computed tomography systems for the detection of vertical root fractures. J Endod 2010;36:126–9.

21. Vasconcelos KF, Nicolielo LF, Nascimento MC, et al. Artefact expression associated with several cone-beam computed tomographic machines when imaging root filled teeth. Int Endod J 2015;48:994–1000.
22. Pinto MG, Rabelo KA, Sousa Melo SL, et al. Influence of exposure parameters on the detection of simulated root fractures in the presence of various intracanal materials. Int Endod J 2017;50:586–94.
23. Neves FS, Freitas DQ, Campos PS, et al. Evaluation of cone-beam computed tomography in the diagnosis of vertical root fractures: the influence of imaging modes and root canal materials. J Endod 2014;40:1530–6.
24. Melo SL, Haiter-Neto F, Correa LR, et al. Comparative diagnostic yield of cone beam CT reconstruction using various software programs on the detection of vertical root fractures. Dentomaxillofac Radiol 2013;42:20120459.
25. Ozer SY. Detection of vertical root fractures by using cone beam computed tomography with variable voxel sizes in an *in vitro* model. J Endod 2011; 37:75–9.
26. Amintavakoli N. *The Effect of Cone Beam CT Voxel Size on the Identification of Vertical and Horizontal Root Fractures: An* In-vitro *Study* [MSc thesis]. Toronto, ON, Canada: University of Toronto; 2013.
27. Fox A, Basrani B, Kishen A, Lam EW. A novel method for characterizing beam hardening artifacts from cone beam CT images. J Endod 2018. Accepted for publication.
28. Krupinski E, Tillack A, Richter L, et al. Eye-movement study and human performance using using telepathology virtual slides. Implications for medical education and differences with experience. Hum Pathol 2006;37:1543–56.